Supplementary information

Realizing high thermoelectric performance in GeTe by defect engineering on cation sites

Can Zhu[a], Feng Luo[a], Jian Wang[a], Shun Zhang[a], Jiafu Wang[a], Hongxia Liu[b,c,*], Zhigang Sun[a,b,c,*]

[a] *State Key Laboratory of Advanced Technology for Materials Synthesis and Processing, Wuhan University of Technology, Wuhan 430070, China.*

[b] *School of Materials Science & Engineering, Taiyuan University of Science and Technology, Taiyuan 030024, China.*

[c] *Laboratory of Magnetic and Electric Functional Materials and the Applications, The Key Laboratory of Shanxi Province, Taiyuan 030024, China.*

* Corresponding author.

E-mail address: sun_zg@whut.edu.cn (Prof. Zhigang Sun) and hongxliu@126.com (Dr. Hongxia Liu)

1. First-principles calculation methods

The path to calculate band structure for rhombohedral and cubic GeTe is P–Γ–L–B–F–B_1–Z–Γ–X and K–Γ–L–U–W–X–W–U–L–Γ–K, respectively. The coordinates of high-symmetry points in the Brillion zone are derived from the developed framework,[1] as shown in **Table.S1**. The maximum and secondary valance bands of GeTe-based materials, as well as the minimum conduction band, are important factors for thermoelectric properties. Therefore, parts of the band structures on the path of P–Γ–L–B (rhombohedral GeTe) and K–Γ–L–U–X (cubic GeTe)[2] containing these features are shown in Fig.1.

Table.S1 Coordinates of high-symmetry points in Brillion zone of rhombohedral and cubic GeTe

rhombohedral GeTe		cubic GeTe	
P	(0.756, 0.372, 0.372)	K	(0.375, 0.375, 0.75)
Γ	(0, 0, 0)	Γ	(0, 0, 0)
L	(0.5, 0, 0)	L	(0.5, 0.5, 0.5)
B	(0.756, 0.5, 0.244)	U	(0.625, 0.25, 0.625)
F	(0.5, 0.5, 0)	W	(0.5, 0.25, 0.75)
B_1	(0.5, 0.244, -0.244)	X	(0.5, 0, 0.5)
Z	(0.5, 0.5, 0.5)		
X	(0.372, 0, -0.372)		

2. Phase structures

2.1 XRD patterns

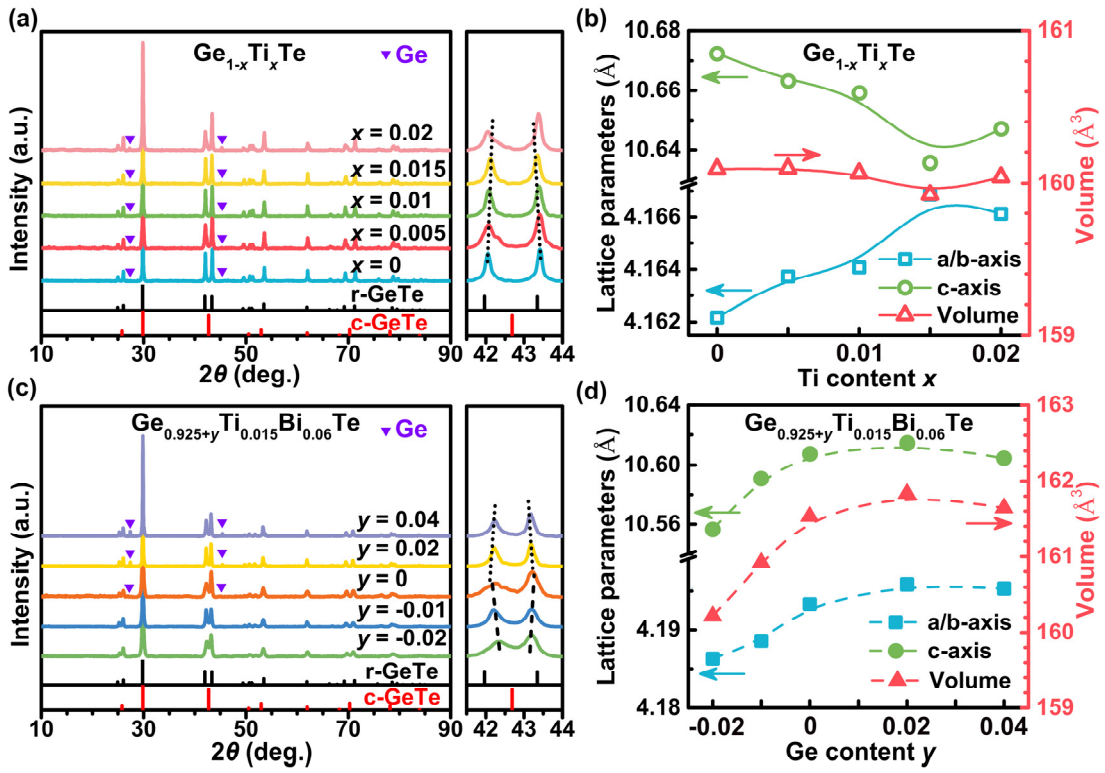

Fig.S1 The XRD patterns of (a) $Ge_{1-x}Ti_xTe$ (x = 0, 0.005, 0.01, 0.015, 0.02) series and (c) $Ge_{0.925+y}Ti_{0.015}Bi_{0.06}Te$ (y = -0.02, -0.01, 0, 0.02, 0.04) series at RT. Composition dependent lattice parameters and volume for (b) $Ge_{1-x}Ti_xTe$ and (d) $Ge_{0.925+y}Ti_{0.015}Bi_{0.06}Te$ series based on the hexagonal unit cell at RT.

2.2 Lattice parameters for hexagonal, trigonal, and pseudo cubic GeTe unit cells

When describing the crystal structures of the rhombohedral GeTe, all three different lattice parameters / interaxial angles based on hexagonal,[3-6] trigonal,[7-9] and pseudo cubic[10-14] GeTe unit cells are often used. As shown in **Fig.S2**(a), the hexagonal GeTe unit cell has lattice parameters a and c, the trigonal GeTe unit cell has lattice parameter a_2 and interaxial angle α_2, and the pseudo cubic GeTe unit cell has lattice parameter a_1 and interaxial angle α_1. The coordinate of one kind of atom in a hexagonal unit cell is (0, 0, 0), (2/3, 1/3, 1/3), and (1/3, 2/3, 2/3). According to the coordinate

transformation from hexagonal coordinate to rectangular coordinate (**Fig.S2**(b)), the lattice parameters and interaxial angles based on the other two unit cells can be calculated according to the following formulas: $a_2 = |\overrightarrow{OA}|$, $a_1 = |\overrightarrow{OE}|$, $\cos\alpha_2 = \frac{\overrightarrow{OA}\cdot\overrightarrow{OB}}{|\overrightarrow{OA}||\overrightarrow{OB}|}$, and $\cos\alpha_1 = \frac{\overrightarrow{OE}\cdot\overrightarrow{OF}}{|\overrightarrow{OE}||\overrightarrow{OF}|}$, see **Table.S2**.

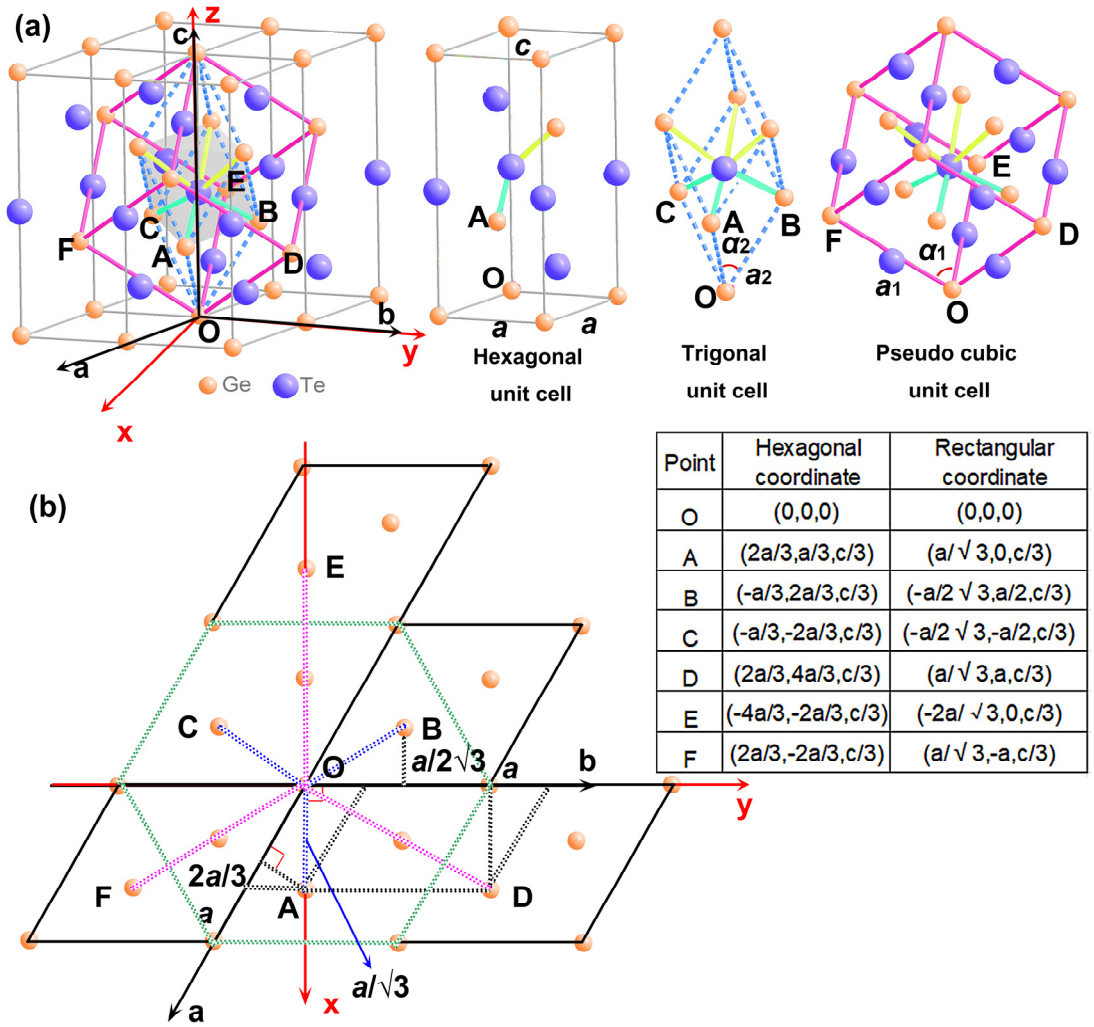

Point	Hexagonal coordinate	Rectangular coordinate
O	(0,0,0)	(0,0,0)
A	(2a/3,a/3,c/3)	(a/√3,0,c/3)
B	(-a/3,2a/3,c/3)	(-a/2√3,a/2,c/3)
C	(-a/3,-2a/3,c/3)	(-a/2√3,-a/2,c/3)
D	(2a/3,4a/3,c/3)	(a/√3,a,c/3)
E	(-4a/3,-2a/3,c/3)	(-2a/√3,0,c/3)
F	(2a/3,-2a/3,c/3)	(a/√3,-a,c/3)

Fig.S2 (a) The crystal structures of GeTe in hexagonal coordinate system O-*abc* (black axes) and rectangular coordinate system O-*xyz* (red axes), and the hexagonal, trigonal, and pseudo cubic GeTe unit cells. (b) Projection of the lattice on the *ab*/*xy* plane and the corresponding coordinates in two coordinate systems. OA, OB, and OC are the projection of trigonal GeTe's edges and OD, OE, and OF are the projection of pseudo cubic GeTe's edges.

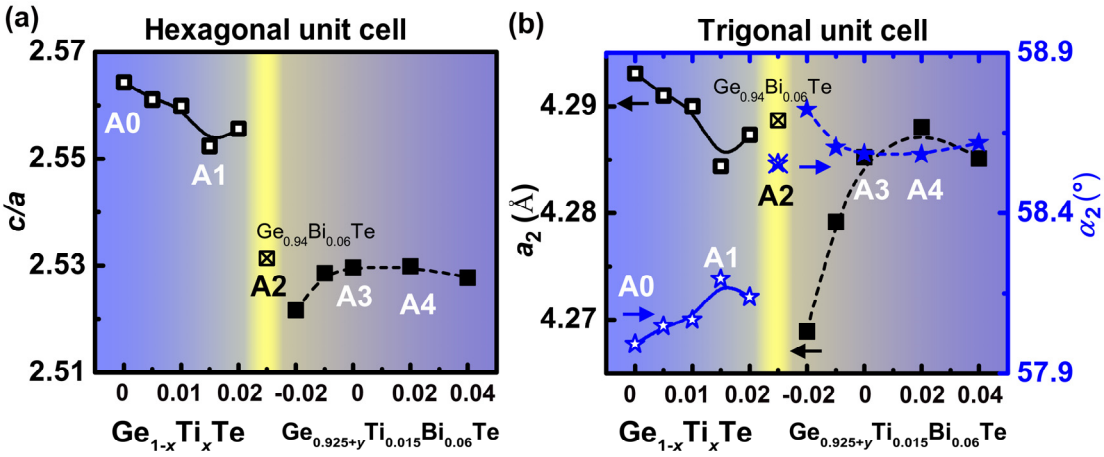

Fig.S3 Composition-dependent (a) lattice parameters ratio (c/a) based on hexagonal unit cell, and (b) lattice parameter a_2 and interaxial angle α_2 based on trigonal unit cell.

Table.S2 The lattice parameters of samples in this work based on hexagonal, trigonal, and pseudo cubic unit cells at room temperature

Samples		Hexagonal unit cell				Trigonal unit cell		Pseudo cubic unit cell	
		a (Å)	c (Å)	c/a	V (Å^3)	a_2 (Å)	α_2 (°)	a_1 (Å)	α_1 (°)
$Ge_{1-x}Ti_xTe$									
$x = 0$	A0	4.1622	10.6725	2.5642	160.092	4.2931	57.99	5.9795	88.23
$x = 0.005$		4.1637	10.6631	2.5610	160.095	4.2910	58.05	5.9790	88.28
$x = 0.01$		4.1641	10.6592	2.5598	160.064	4.2900	58.07	5.9786	88.29
$x = 0.015$	A1	4.1669	10.6357	2.5524	159.924	4.2844	58.19	5.9765	88.41
$x = 0.02$		4.1661	10.6471	2.5556	160.039	4.2873	58.14	5.9781	88.36
$Ge_{0.94}Bi_{0.06}Te$	A2	4.1947	10.6183	2.5314	161.805	4.2887	58.56	5.9990	88.73
$Ge_{0.925+y}Ti_{0.015}Bi_{0.06}Te$									
$y = -0.02$		4.1863	10.5565	2.5217	160.218	4.2689	58.72	5.9790	88.88
$y = -0.01$		4.1886	10.5909	2.5285	160.918	4.2792	58.60	5.9880	88.77
$y = 0$	A3	4.1933	10.6074	2.5296	161.531	4.2852	58.59	5.9956	88.76
$y = 0.02$	A4	4.1958	10.6145	2.5298	161.834	4.2880	58.58	5.9993	88.76
$y = 0.04$		4.1953	10.6046	2.5277	161.642	4.2851	58.62	5.9969	88.79

Trigonal unit cell	Pseudo cubic unit cell
$a_2 = \frac{\sqrt{3a^2 + c^2}}{3}$	$a_1 = \frac{\sqrt{12a^2 + c^2}}{3}$
$\cos\alpha_2 = \frac{\left\lvert \frac{c^2}{9} - \frac{a^2}{6} \right\rvert}{a_2^2}$	$\cos\alpha_1 = \frac{\left\lvert \frac{c^2}{9} - \frac{2a^2}{3} \right\rvert}{a_1^2}$
or	or
$\sin\frac{\alpha_2}{2} = \frac{3}{2}\frac{1}{\sqrt{3 + \left(\frac{c}{a}\right)^2}}$	$\sin\frac{\alpha_1}{2} = \frac{3}{2}\frac{1}{\sqrt{3 + \left(\frac{c}{2a}\right)^2}}$

3. Microstructure

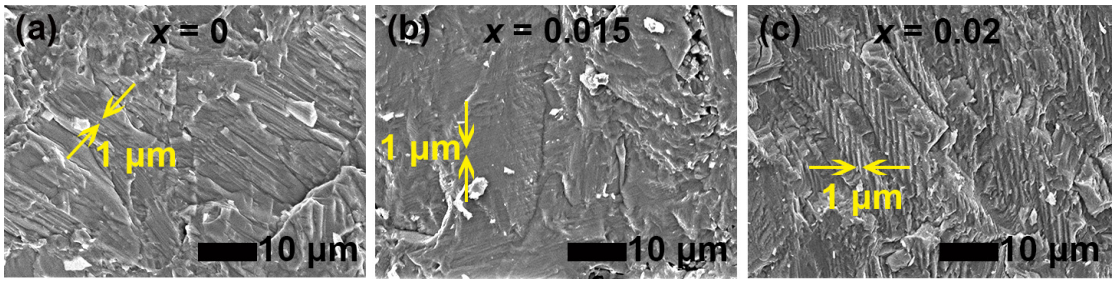

Fig.S4 SEM images of the fractured surfaces of $Ge_{1-x}Ti_xTe$ (x = 0, 0.015, 0.02) series.

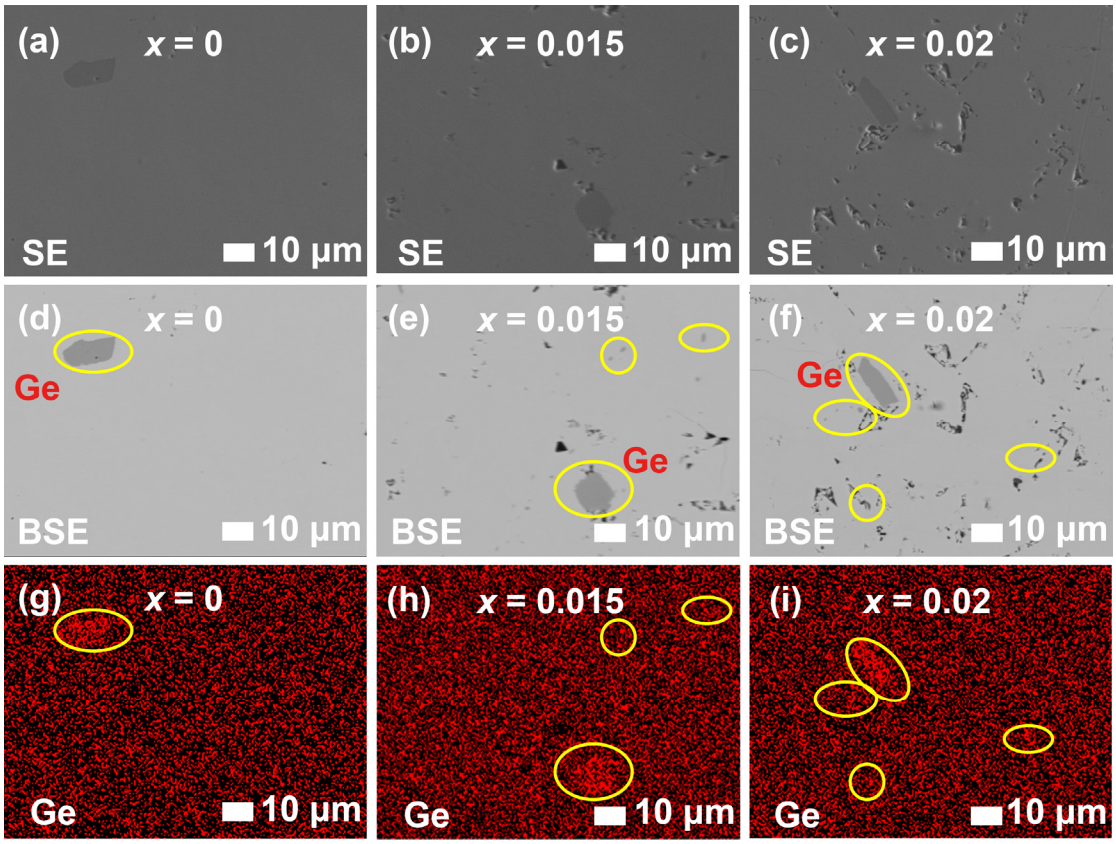

Fig.S5 SE, BSE and Ge-mapping images of the polished surfaces for $Ge_{1-x}Ti_xTe$ (x = 0, 0.015, 0.02).

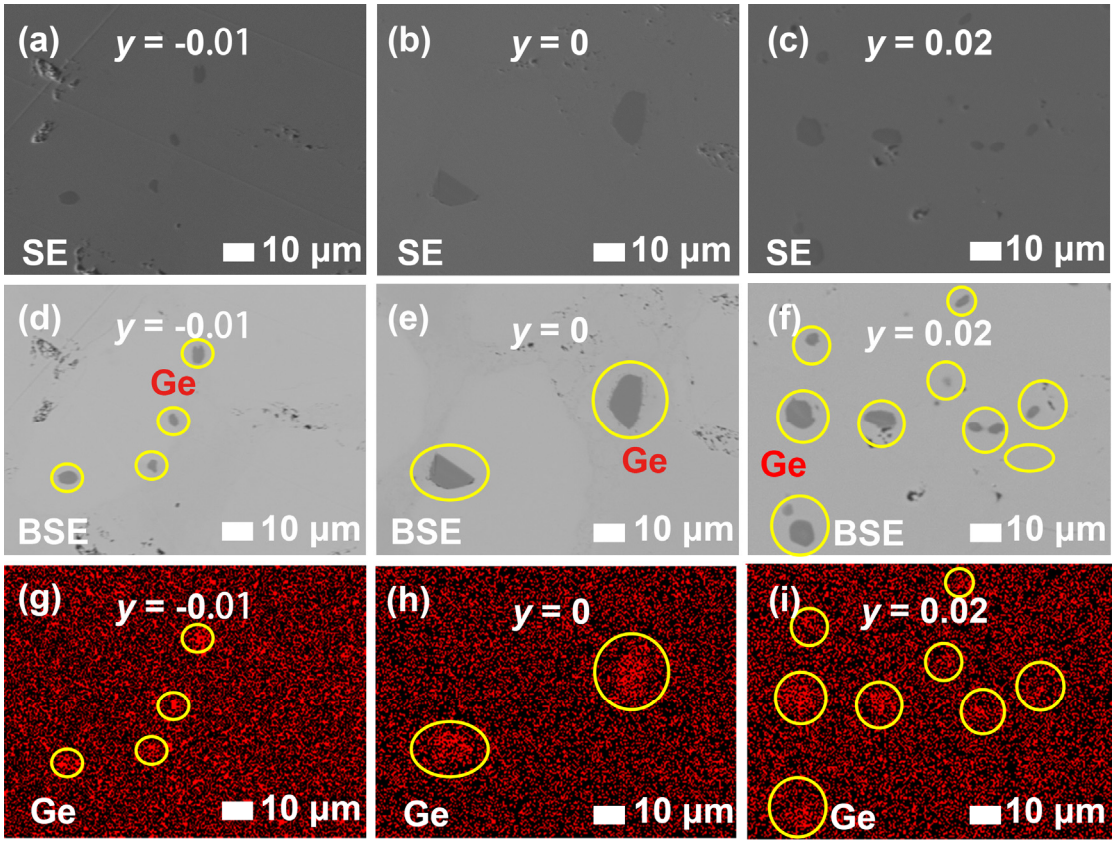

Fig.S6 SE, BSE and Ge-mapping images of the polished surfaces for $Ge_{0.925+y}Ti_{0.015}Bi_{0.06}Te$ (y = -0.01, 0, 0.02).

4. Thermoelectric properties

4.1 Electronic transport properties

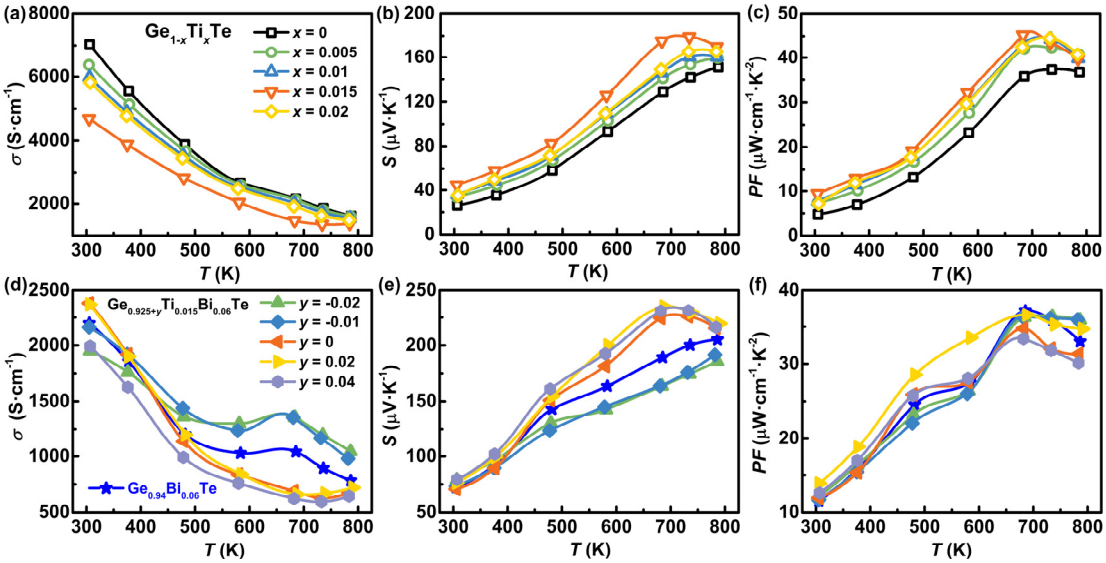

Fig.S7 The temperature-dependent (a, d) conductivity σ, (b, e) Seebeck coefficient S, and (c, f) power factor PF of $Ge_{1-x}Ti_xTe$ series and $Ge_{0.925+y}Ti_{0.015}Bi_{0.06}Te$ series, respectively.

4.1.1 Single parabolic band model

Based on the single parabolic band (SPB) approximation, the effective mass m^* can be derived by:[15, 16]

$$F_j(\eta) = \int_0^{\infty} \frac{\varepsilon^j}{1+exp(\varepsilon-\eta)} d\varepsilon \tag{S1}$$

$$S = \pm \frac{k_B}{e}\left[\frac{(r+5/2)F_{r+3/2}(\eta)}{(r+3/2)F_{r+1/2}(\eta)} - \eta\right] \tag{S2}$$

$$m^* = \frac{h^2}{2k_B T}\left[\frac{n}{4\pi F_{1/2}(\eta)}\right]^{2/3} \tag{S3}$$

$F_j(\eta)$ is the Fermi integral function and $\eta = E_F/k_BT$, which is related to the carrier concentration n. As it is considered that the GeTe-based materials basically obey phonon-dominated scattering, the scattering factor r = -1/2 is always taken.[5, 16]

Table.S3 The electronic transport parameters of samples in this work at room temperature

Samples		n_H(10^{20} cm^{-3})	μ_H(cm^2·V^{-1}·s^{-1})	σ S·cm^{-1})	S (μV·K^{-1})	m^*/m_0
$Ge_{1-x}Ti_xTe$						
x = 0	A0	8.21	52.59	7032.02	26.12	1.1319
x = 0.005		8.01	46.09	6461.60	33.36	1.4162
x = 0.01		7.80	43.27	6077.52	35.15	1.4646
x = 0.015	A1	7.08	39.42	4745.08	43.87	1.7068
x = 0.02		8.08	42.11	5926.92	33.61	1.4349
$Ge_{0.94}Bi_{0.06}Te$	A2	3.85	40.86	2218.57	71.28	1.8535
$Ge_{0.925+y}Ti_{0.015}Bi_{0.06}Te$						
y = -0.02		5.75	20.08	1964.32	77.58	2.6486
y = -0.01		5.32	25.67	2177.20	72.44	2.3387
y = 0	A3	3.25	49.72	2415.30	70.18	1.6286
y = 0.02	A4	3.00	52.64	2410.81	75.03	1.6566
y = 0.04		2.81	45.37	2024.90	78.04	1.6537

Since both S and σ are the function of carrier concentration and are related to each other, the transport coefficients σ_{E0} and the weighted mobility μ_W are introduced to describe the intrinsic transport properties of materials.[5, 17] And they can be expressed as:

$$\sigma = \sigma_{E_0} \ln(1 + e^{\eta}) \tag{S4}$$

$$\sigma_{E_0} = \frac{2^{9/2} e\pi (m_e k_B T)^{3/2}}{3h^3} \mu_W \tag{S5}$$

$$\mu_W = \mu_0 \left(\frac{m^*}{m_e}\right)^{3/2} \tag{S6}$$

And k_B, h, and η are the Boltzmann constant, Planck constant, and the reduced Fermi level. It can be seen from the above formulas that the parameter σ_{E0} is a conductivity expression independent of the carrier concentration, which excludes the error of the carrier concentration in the Hall measurement. The σ_{E0} characterizes how well a

material conducts electricity for a given η (*i.e.*, at a given n). The larger σ_{E0} generally reflects the good crystallinity of the material. The parameter σ_{E0} can be expressed by the weighted mobility μ_W, which is closely related to the effective mass. Therefore, the change in μ_W can also explain the relationship between S and σ, and the μ_W can initially reflect the scale of PF.

The κ_e is calculated according to the Wiedemann–Franz law $\kappa_e = L\sigma T$, where L is the Lorenz number based on the SPB approximation:[15, 18]

$$L = \left(\frac{k_B}{e}\right)^2 \left\{ \frac{(r+7/2)F_{r+5/2}(\eta)}{(r+3/2)F_{r+1/2}(\eta)} - \left[\frac{(r+5/2)F_{r+3/2}(\eta)}{(r+3/2)F_{r+1/2}(\eta)}\right]^2 \right\} \quad \text{(S7)}$$

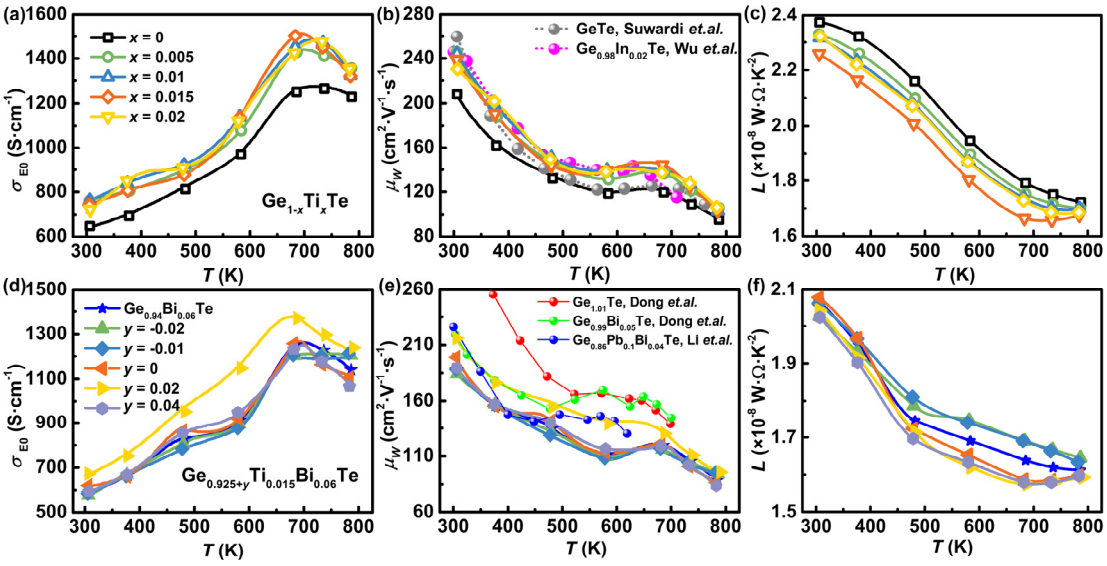

Fig.S8 The temperature-dependent (a, d) transport coefficients σ_{E0}, (b, e) weighted mobility μ_W, and (c, f) Lorenz number L of $Ge_{1-x}Ti_xTe$ series and $Ge_{0.925+y}Ti_{0.015}Bi_{0.06}Te$ series, respectively. The μ_W is compared with the doped-GeTe[17, 19] and other works[10, 20] in (b) and (e).

4.2 Thermal transport properties

Table.S4 The heat capacity C_p and density ρ used for each sample in this work

$Ge_{1-x}Ti_xTe$				$Ge_{0.925+y}Ti_{0.015}Bi_{0.06}Te$			
x		C_p ($J\cdot g^{-1}\cdot K^{-1}$)	ρ ($g\cdot cm^{-3}$)	y		C_p ($J\cdot g^{-1}\cdot K^{-1}$)	ρ ($g\cdot cm^{-3}$)
0	A0	0.2491	6.11	-0.02		0.2391	6.16
0.005		0.2493	6.02	-0.01		0.2394	6.21
0.01		0.2494	6.02	0	A3	0.2398	6.15
0.015	A1	0.2496	5.93	0.02	A4	0.2405	6.12
0.02		0.2498	5.97	0.04		0.2412	6.13
$Ge_{0.94}Bi_{0.06}Te$	A2	0.2394	6.13				

4.2.1 Debye–Callaway model for calculating the lattice thermal conductivity

According to the Debye–Callaway model,[21-24] κ_L can be defined as a sum of the spectral lattice thermal conductivity $\kappa_S(f)$ from different frequencies (f):

$$\kappa_L = \int \kappa_S(f)\, df = \frac{1}{3}\int_0^{f_D} C_S(f) v_g(f)^2 \tau_{tot}(f)\, df \tag{S8}$$

The $\kappa_S(f)$ is determined by the spectral heat capacity $C_S(f)$, the phonon group velocity $v_g(f)$, and the total relaxation time $\tau_{tot}(f)$. For simple approximation, $v_g(f)$ is assumed as a constant value v_s (sound velocity). The Debye frequency f_D can be expressed as:

$$f_D = \frac{k_B \theta_D}{\hbar} = \left(\frac{6\pi^2 N}{V}\right)^{1/3} v_s \tag{S9}$$

where θ_D is Debye temperature, N is the number of atoms in a unit cell volume, V is the unit-cell volume, k_B is the Boltzmann constant and $\hbar$ is the reduced Plank constant. The $C_S(f)$ can be expressed as:

$$C_S(f) = \frac{3 k_B f^2}{2\pi^2 {v_s}^3} \tag{S10}$$

Thus, κ_L and κ_S are calculated by

$$\kappa_L = \frac{k_B}{2\pi^2 v_s}\left(\frac{k_B T}{\hbar}\right)^3 \int_0^{\theta_D/T} \tau_{tot}(x) \frac{x^4 \exp(x)}{[\exp(x)-1]^2} dx \tag{S11}$$

$$\kappa_S = \frac{k_B}{2\pi^2 v_s}\left(\frac{k_B T}{\hbar}\right)^3 \tau_{tot}(x)\frac{x^4 \exp(x)}{[\exp(x)-1]^2} \quad \text{(S12)}$$

where $x = \hbar f / k_B T$ is the reduced phonon frequency. According to Matthiessen's rule,[25] $\tau_{tot}(x)$ is the reciprocal sum of the relaxation times from different phonon scattering mechanisms including the Umklapp phonon-phonon scatterings (U), normal phonon-phonon scatterings (N), grain boundaries scatterings (B), point defects scatterings (PD), nano-precipitates phonon scatterings (NP) and stacking fault phonon scatterings (SF). So, τ_{tot} is calculated by

$$\tau_{tot}^{-1} = \tau_U^{-1} + \tau_N^{-1} + \tau_B^{-1} + \tau_{PD}^{-1} + \tau_{NP}^{-1} + \tau_{SF}^{-1} + \cdots \quad \text{(S13)}$$

The τ_U^{-1} is calculated by

$$\tau_U^{-1} = \frac{\hbar \gamma^2 f^2 T}{M_{av} v_s^2 \theta_D}\exp\left(-\frac{\theta_D}{3T}\right) \quad \text{(S14)}$$

where M_{av} and γ are the average atomic mass and Grüneisen parameter respectively. The τ_N^{-1} can be simply expressed as τ_U^{-1} with an additional factor β, as

$$\tau_N^{-1} = \beta \tau_U^{-1} \quad \text{(S15)}$$

The τ_B^{-1} is calculated by

$$\tau_B^{-1} = \frac{v_s}{D} \quad \text{(S16)}$$

where D is the average grain size of polycrystalline materials.

The τ_{PD}^{-1} is calculated by

$$\tau_{PD}^{-1} = \frac{V_{av} f^4}{4\pi v_s^3}\Gamma \quad \text{(S17)}$$

where V_{av} is the average atomic volume. The disorder scattering parameter $\Gamma = \Gamma_M + \Gamma_S$ describes the mass and atomic size contrast with the lattice, which are calculated by[26, 27]

$$\Gamma_{\mathrm{M}} = \frac{\sum_{i=1}^{n} c_i \left(\frac{M_{\mathrm{av}i}}{M_{\mathrm{av}}}\right)^2 f_i^1 f_i^2 \left(\frac{M_i^1 - M_i^2}{M_{\mathrm{av}i}}\right)^2}{\sum_{i=1}^{n} c_i} \tag{S18}$$

$$\Gamma_{\mathrm{S}} = \frac{\sum_{i=1}^{n} c_i \left(\frac{M_{\mathrm{av}i}}{M_{\mathrm{av}}}\right)^2 f_i^1 f_i^2 \varepsilon_i \left(\frac{r_i^1 - r_i^2}{r_{\mathrm{av}i}}\right)^2}{\sum_{i=1}^{n} c_i} \tag{S19}$$

where n is the number of sublattices, c_i, $M_{\mathrm{av}i}$ and $r_{\mathrm{av}i}$ are the relative fraction, average mass, and atomic radius for the ith sublattice respectively. For GeTe, there are two different sublattices (the Ge site and the Te site); thus, $n = 2$ and $c_1 = c_2 = 1$. The M_i^j, r_i^j, and f_i^j represent the jth atomic mass, atomic radius, and atomic fraction on the ith sublattice, respectively.

The τ_{NP}^{-1} is calculated by[28, 29]

$$\tau_{\mathrm{NP}}^{-1} = v_{\mathrm{s}} \left[\left(2\pi {R_{\mathrm{NP}}}^2\right)^{-1} + \left(\pi {R_{\mathrm{NP}}}^2 \frac{4}{9} \left(\frac{\Delta\rho}{\rho}\right)^2 \left(\frac{f R_{\mathrm{NP}}}{v_{\mathrm{s}}}\right)^4\right)^{-1} \right]^{-1} N_{\mathrm{NP}} \tag{S20}$$

where R_{NP} and N_{NP} are the radius and number density for the nano-precipitates, ρ and $\Delta\rho$ are the matrix density and density difference between the precipitate and matrix.

The τ_{SF}^{-1} is calculated by[30]

$$\tau_{\mathrm{SF}}^{-1} = 0.7 \frac{a^2}{v_{\mathrm{s}}} \gamma^2 f^2 N_{\mathrm{SF}} \tag{S21}$$

where a is the lattice parameter based on c-GeTe and N_{SF} is the number of stacking faults induced by herringbones domain boundaries[23] or planar vacancies[28] crossing a line of unit length. The parameters for modelling κ_{L} in this work are shown in **Table.S5** and **Table.S6**.

Table.S5 Parameters for modelling the lattice thermal conductivity

Parameters	Values
Grüneisen parameter γ	1.56[31]
Sound velocity v_s (m·s^{-1})	1967[31]
Debye temperature θ_D (K)	194.88
Lattice parameter a (Å)	5.986
Average atomic mass M_{av} (kg)	1.6625×10^{-25}
Grain size D (μm)	50
Matrix density ρ (g·cm^{-3})	6.0[28]
Density difference between matrix and precipitates $\Delta\rho$ (g·cm^{-3})	0.7[28]
Radius for the nano-precipitates Ge R_{NP} (nm)	55[6]
Number density of nano-precipitates N_{NP} (m^{-3})	3×10^{18} [ref28]
Number of stacking faults crossing a line of unit length N_{SF} (m^{-1})	1×10^{6} (fitted)

Table.S6 Parameters for modelling point defect scattering. Based on the elasticity theory,[32, 33] the longitudinal/transverse sound velocity $v_i = a(\delta/M_{av})^{1/2}$, where δ is the force constant in the lattice. The a and δ are assumed to be constant because of the same structure. The average sound velocity $v_s = [(2v_t^{-3} + v_l^{-3})/3]^{-1/3}$.

Samples	M_{av} (10^{-25} kg)	v_t (m·s^{-1})	v_l (m·s^{-1})	v_s (m·s^{-1})	θ_D (K)	Γ
GeTe	1.6625	1780[31]	2930[31]	1967[31]	194.88	0
$Ge_{0.995}Ti_{0.005}Te$	1.6614	1780.55	2930.90	1967.29	194.91	0.00964
$Ge_{0.99}Ti_{0.01}Te$	1.6604	1781.10	2931.81	1967.90	194.97	0.01912
$Ge_{0.985}Ti_{0.015}Te$	1.6594	1781.65	2932.72	1968.51	195.03	0.02844
$Ge_{0.98}Ti_{0.02}Te$	1.6583	1782.21	2933.63	1969.12	195.09	0.03761
$Ge_{0.94}Bi_{0.06}Te$	1.7304	1744.71	2871.92	1927.70	190.99	0.085 (fitted)
$Ge_{0.925}Ti_{0.015}Bi_{0.06}Te$	1.7273	1746.27	2874.48	1929.42	191.16	0.15 (fitted)
$Ge_{0.945}Ti_{0.015}Bi_{0.06}Te$	1.7394	1740.21	2864.50	1922.72	190.49	0.17 (fitted)

4.2.2 Cahill–Watson–Pohl (CWP) model for calculating the minimum lattice thermal conductivity

The lower limit to the lattice thermal conductivity of this model κ_{CWP} is derived from the Einstein's random-walk model, but replacing Einstein temperature/frequency

with oscillators defined within the Debye model, which can be calculated as shown below:[34]

$$\kappa_{\mathrm{Lmin}} = \kappa_{\mathrm{CWP}} = \frac{k_{\mathrm{B}}}{2\pi^2 v_{\mathrm{S}}}\left(\frac{k_{\mathrm{B}}T}{\hbar}\right)^3 \int_0^{\theta_{\mathrm{D}}/T} \frac{\pi}{f}\frac{x^4\exp(x)}{[\exp(x)-1]^2}dx \tag{S22}$$

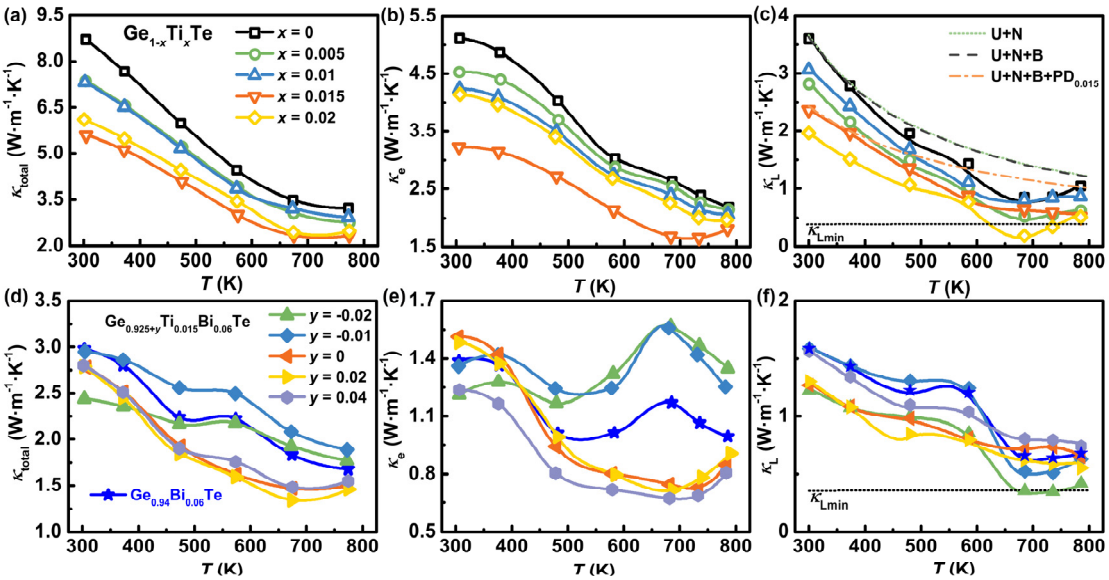

Fig.S9 The temperature-dependent (a, d) total thermal conductivity κ_{total}, (b, e) electronic thermal conductivity κ_{e}, and (c, f) lattice thermal conductivity κ_{L} of $Ge_{1-x}Ti_xTe$ series and $Ge_{0.925+y}Ti_{0.015}Bi_{0.06}Te$ series, respectively.

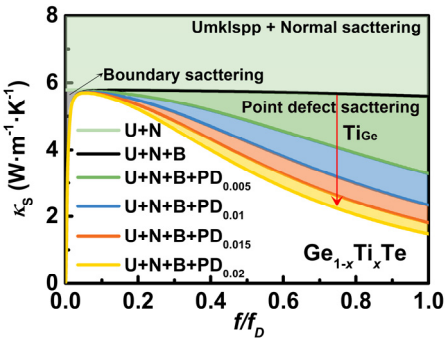

Fig.S10 The spectral lattice thermal conductivity (κ_{S}) as a function of phonon frequency (f) based on different scatterings of $Ge_{1-x}Ti_xTe$ series.

4.3 Quality factor *B* and *ZT*

The *ZT* can treated as a function of two independent variables: η (reduced electron chemical potential) and the material quality factor *B*. The η is related to doping and temperature, but *B* just dependent on temperature and retains only the inherent material properties that determine *ZT*:[35]

$$B = \left(\frac{k_B}{e}\right)^2 \frac{\sigma_{E_0}}{\kappa_L} T \tag{S23}$$

Above all, *ZT* can be calculated by the η–dependent parameters:[35]

$$ZT = \frac{S^2 \sigma T}{\kappa_L + \kappa_e} = \frac{S^2}{\frac{\kappa_L}{\sigma T} + L} = \frac{S^2(\eta)}{\frac{\kappa_L}{\sigma_{E_0} \ln(1+e^{\eta}) T} + L(\eta)} = \frac{S^2(\eta)}{\frac{\left(\frac{k_B}{e}\right)^2}{B \ln(1+e^{\eta})} + L(\eta)} \tag{S24}$$

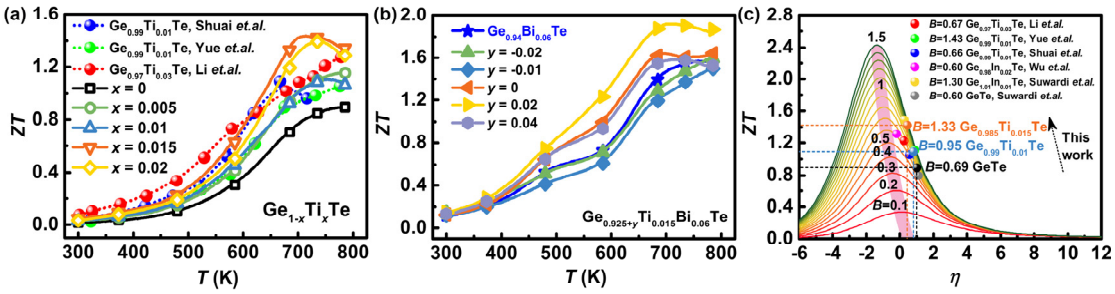

Fig.S11 The temperature-dependent *ZT* of (a) $Ge_{1-x}Ti_xTe$ series compared with Ti-doping samples in references,[3, 36, 37] and (b) $Ge_{0.925+y}Ti_{0.015}Bi_{0.06}Te$ series. (c) The ZT_{max} vs. η relation of $Ge_{1-x}Ti_xTe$ at different *B*, compared with other works.[3, 17, 19, 36, 37]

4.4 Repeated thermoelectric properties measurement

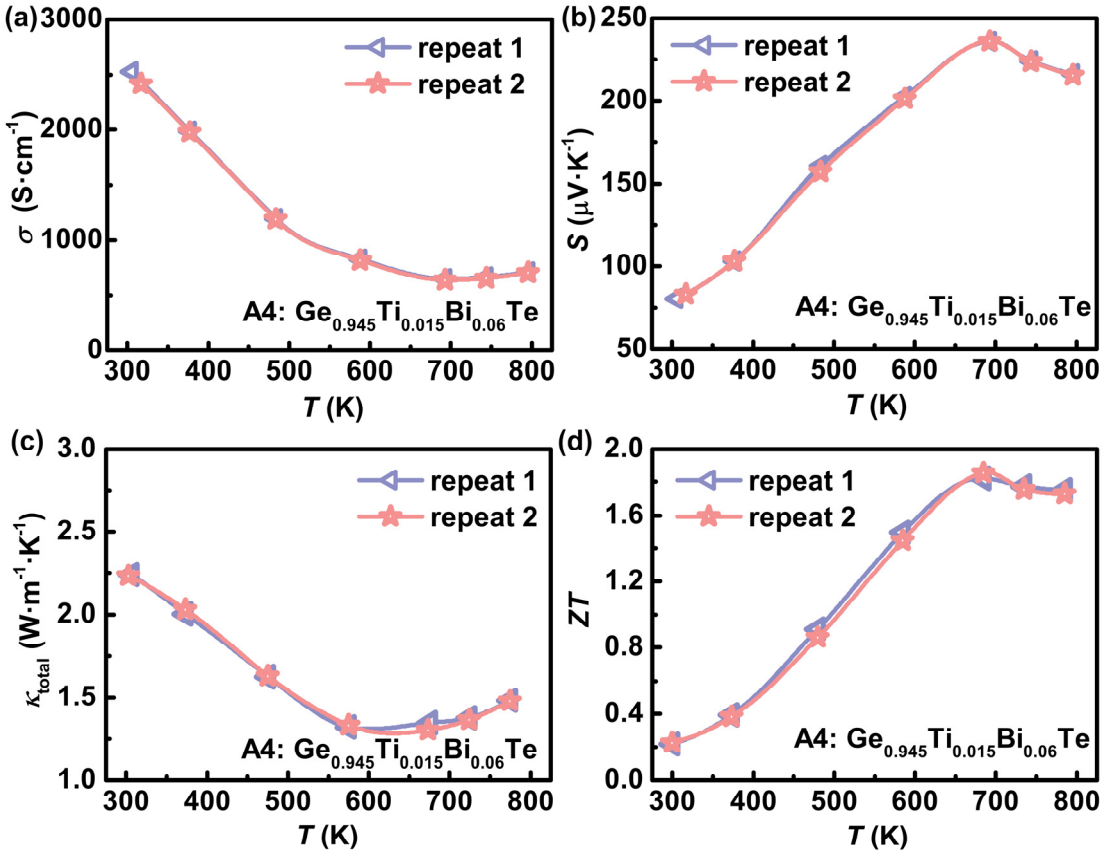

Fig.S12 The temperature-dependent (a) σ, (b) S, (c) κ_{total}, and (d) ZT for the repeated thermoelectric properties measurement for the A4 sample.

References:

1. W. Setyawan and S. Curtarolo, *Comput. Mater. Sci.*, 2010, **49**, 299-312.
2. M. Hong, J. Zou and Z. G. Chen, *Adv. Mater.*, 2019, **31**, 1807071.
3. J. Shuai, X. J. Tan, Q. Guo, J. T. Xu, A. Gellé, R. Gautier, J. F. Halet, F. Failamani, J. Jiang and T. Mori, *Mater. Today Phys.*, 2019, **9**, 100094.
4. R. K. Vankayala, T. W. Lan, P. Parajuli, F. Liu, R. Rao, S. H. Yu, T. L. Hung, C. H. Lee, S.-i. Yano, C. R. Hsing, D. L. Nguyen, C. L. Chen, S. Bhattacharya, K. H. Chen, M. N. Ou, O. Rancu, A. M. Rao and Y. Y. Chen, *Adv. Sci.*, 2020, **7**, 2002494.
5. N. H. Li, W. L. He, C. J. Li, G. W. Wang, G. Y. Wang, X. Y. Zhou and X. Lu, *J. Mater. Chem. A*, 2021, **9**, 2385-2393.
6. Q. Sun, M. Li, X. L. Shi, S. D. Xu, W. D. Liu, M. Hong, W. y. Lyu, Y. Yin, M. Dargusch, J. Zou and Z. G. Chen, *Adv. Energy Mater.*, 2021, **11**, 2100544.
7. X. Y. Zhang, Z. L. Bu, S. Q. Lin, Z. W. Chen, W. Li and Y. Z. Pei, *Joule*, 2020, **4**, 1-18.

8. B. Srinivasan, S. Le Tonquesse, A. Gelle, C. Bourges, L. Monier, I. Ohkubo, J.-F. Halet, D. Berthebaud and T. Mori, *J. Mater. Chem. A*, 2020, **8**, 19805-19821.
9. M. Li, Q. Sun, S.-D. Xu, M. Hong, W.-Y. Lyu, J.-X. Liu, Y. Wang, M. Dargusch, J. Zou and Z.-G. Chen, *Adv. Mater.*, 2021, **33**, 2102575.
10. J. F. Dong, F. H. Sun, H. C. Tang, J. Pei, H. L. Zhuang, H. H. Hu, B. P. Zhang, Y. Pan and J. F. Li, *Energy Environ. Sci.*, 2019, **12**, 1396-1403.
11. Z. Bu, Z. Chen, X. Zhang, S. Lin, J. Mao, W. Li, Y. Chen and Y. Pei, *Mater. Today Phys.*, 2020, **15**, 100260.
12. Y. Jin, D. Y. Wang, Y. T. Qiu and L. D. Zhao, *J. Mater. Chem. C*, 2021, **9**, 6484-6490.
13. L. Wang, J. Li, Y. Xie, L. Hu, F. Liu, W. Ao, J. Luo and C. Zhang, *Mater. Today Phys.*, 2021, **16**, 100308.
14. X. Y. Wang, W. H. Xue, Z. W. Zhang, X. F. Li, L. Yin, C. Chen, B. Yu, J. H. Sui, F. Cao, X. J. Liu, J. Mao, Y. M. Wang, X. Lin and Q. Zhang, *ACS Appl. Mater. Inter.*, 2021, **13**, 45717-45725.
15. H. Naithani and T. Dasgupta, *ACS Appl. Energy Mater.*, 2020, **3**, 2200-2213.
16. L. Xie, Y. J. Chen, R. H. Liu, E. Song, T. Xing, T. T. Deng, Q. F. Song, J. J. Liu, R. K. Zheng, X. Gao, S. Q. Bai and L. D. Chen, *Nano Energy*, 2020, **68**, 104347.
17. A. Suwardi, J. Cao, Y. Zhao, J. Wu, S. W. Chien, X. Y. Tan, L. Hu, X. Wang, W. Wang, D. Li, Y. Yin, W. X. Zhou, D. V. M. Repaka, J. Chen, Y. Zheng, Q. Yan, G. Zhang and J. Xu, *Mater. Today Phys.*, 2020, **14**, 100239.
18. H.-S. Kim, Z. M. Gibbs, Y. Tang, H. Wang and G. J. Snyder, *APL Mater.*, 2015, **3**, 041506.
19. L. H. Wu, X. Li, S. Y. Wang, T. S. Zhang, J. Yang, W. Q. Zhang, L. D. Chen and J. H. Yang, *NPG Asia Mater.*, 2017, **9**, e343.
20. J. Li, X. Y. Zhang, Z. W. Chen, S. Q. Lin, W. Li, J. H. Shen, I. T. Witting, A. Faghaninia, Y. Chen, A. Jain, L. D. Chen, G. J. Snyder and Y. Z. Pei, *Joule*, 2018, **2**, 976-987.
21. J. Callaway and H. C. von Baeyer, *Phys. Rev.*, 1960, **120**, 1149-1154.
22. D. Bessas, I. Sergueev, H. C. Wille, J. Perßon, D. Ebling and R. P. Hermann, *Phys. Rev. B*, 2012, **86**, 224301.
23. Y.-F. Tsai, M.-Y. Ho, P.-C. Wei and H.-J. Wu, *Acta Mater.*, 2022, **222**, 117406.
24. R. Zhang, J. Pei, Z. Shan, W. Zhou, Y. Wu, Z. Han, Y.-H. Zhao, J.-F. Li, Z.-H. Ge and B.-P. Zhang, *Chem. Eng. J.*, 2022, **429**, 132275.
25. B. K. Agrawal and G. S. Verma, *Phys. Rev.*, 1962, **126**, 24-29.
26. J. Yang, G. P. Meisner and L. Chen, *Appl. Phys. Lett.*, 2004, **85**, 1140-1142.
27. Z. Zheng, X. L. Su, R. R. Deng, C. Stoumpos, H. Y. Xie, W. Liu, Y. G. Yan, S. Q. Hao, C. Uher, C. Wolverton, M. G. Kanatzidis and X. F. Tang, *J. Am. Chem. Soc.*, 2018, **140**, 2673-2686.
28. M. Hong, Y. Wang, W. D. Liu, S. Matsumura, H. Wang, J. Zou and Z. G. Chen, *Adv. Energy Mater.*, 2018, **8**, 1801837.
29. N. Mingo, D. Hauser, N. P. Kobayashi, M. Plissonnier and A. Shakouri, *Nano Lett.*, 2009, **9**, 711-715.
30. B. K. Singh, V. J. Menon and K. C. Sood, *Phys. Rev. B*, 2006, **74**, 184302.

31. M. Hong, Z. G. Chen, L. Yang, Y. C. Zou, M. S. Dargusch, H. Wang and J. Zou, *Adv. Mater.*, 2018, **30**, 1705942.
32. X. Y. Zhang and Y. Z. Pei, *npj Quantum Mater.*, 2017, **2**, 68.
33. J. Q. Li, Y. C. Xie, C. X. Zhang, K. Ma, F. S. Liu, W. Q. Ao, Y. Li and C. H. Zhang, *ACS Appl. Mater. Inter.*, 2019, **11**, 20064-20072.
34. D. G. Cahill, S. K. Watson and R. O. Pohl, *Phys. Rev. B*, 1992, **46**, 6131-6140.
35. S. D. Kang and G. J. Snyder, *Nat. Mater.*, 2017, **16**, 252-257.
36. M. Li, M. Hong, X. Tang, Q. Sun, W. Y. Lyu, S. D. Xu, L. Z. Kou, M. Dargusch, J. Zou and Z. G. Chen, *Nano Energy*, 2020, **73**, 104740.
37. L. Yue, W. L. Cui, S. Q. Zheng, Y. Wu, L. J. Wang, P. P. Bai and X. M. Dong, *J. Phys. Chem. C*, 2020, **124**, 5583-5590.